

## Probing the nonstandard top-gluon couplings through $t\bar{t}\gamma\gamma$ production at the LHC

Seyed Mohsen Etesami and Esmat Darvish Roknabadi

*School of Particles and Accelerators, Institute for Research in Fundamental Sciences (IPM)  
P.O. Box 19395-5531, Tehran, Iran*



(Received 11 February 2019; published 17 July 2019)

In this paper, we investigate the anomalous chromoelectric and chromomagnetic dipole moments of the top quark through top pair production in association with two photons at the LHC. We first present the strategy to reconstruct this process assuming a different source for background processes. Then, we focus on the existing constraints from inclusive top-pair production from the Tevatron and LHC, adding the new LHC measurement. Afterwards, we introduce the new cross section ratio  $R_{2\gamma/\gamma} = \sigma_{t\bar{t}\gamma\gamma}/\sigma_{t\bar{t}\gamma}$  and show the usefulness of this ratio in canceling most of the systematic uncertainties and its special ability to constrain dipole moments. Finally, we use the scalar sum of the transverse momentum of jets  $H_T$  in order to define a signal-dominated region and obtain limits on these anomalous top couplings using different amounts of expected data from the LHC.

DOI: [10.1103/PhysRevD.100.015023](https://doi.org/10.1103/PhysRevD.100.015023)

### I. INTRODUCTION

The top quark is to date the heaviest observed elementary particle [1]. Therefore, from the theoretical point of view it plays an important role in the electroweak symmetry breaking (EWSB) mechanism as it has the largest Yukawa coupling among all of the fundamental particles. Furthermore, the top sector is considered one of the most likely places that new physics can be probed. There are several models that predict the existence of new particles that are expected to preferentially couple to the top quark. Another attractive aspect of the top quark is the  $CP$  properties of its interactions with the standard model (SM) fields.  $CP$  violation has a tiny contribution in the SM model through the complex phase of the Cabibbo-Kobayashi-Maskawa matrix, which is not big enough to explain the observed matter-antimatter asymmetry in the Universe and needs a new source of  $CP$  violation which should come from beyond the SM (BSM). The  $CP$ -violating terms in the top-quark interactions from BSM physics can appear as electric dipole moment (EDM), chromo-EDM (CEDM), and weak EDM terms. Therefore, the precise measurement of these moments will pave the way for finding the effects of new physics.

The first and second runs of the LHC with center-of-mass energies of 7, 8, and 13 TeV confirmed the SM

model of particle physics by discovering the long sought-after Higgs boson [2,3], but no hint of BSM physics has been found. However, there are many SM properties that have not been measured accurately yet. Therefore, one of the missions of the phase II upgrade of the LHC is to make these measurements precise by providing an unprecedented amount of data, which is ultimately expected to be  $3 \text{ ab}^{-1}$  of integrated luminosity (IL). In this context, many rare SM processes become accessible, such as multiboson processes (like  $VVV$  and  $VVVV$ ) and the associated production of top-quark pairs with multibosons (like  $t\bar{t} + VV$  processes, where  $V$  stands for  $W$ ,  $Z$ , or  $\gamma$ ). These processes with multiple fermionic and bosonic degrees of freedom provide a rich ground for testing the SM and BSM couplings such as fermion-gauge boson couplings as well as multiple couplings of gauge bosons. Even though the production phase space of these processes is limited due to the higher energy threshold (which leads to lower cross sections), they benefit from multiplications of final-state particles which significantly reduce background contributions. It should be mentioned that the cross sections of  $t\bar{t}W$ ,  $t\bar{t}Z$ , and  $t\bar{t}\gamma$  processes have been measured by the CMS and ATLAS collaborations [6–10].

The aim of this paper is to study how well the chromoelectric and magnetic dipole moments of the top quark can be measured during top quark pair production in association with two photons,  $t\bar{t}\gamma\gamma$ . As these dipole moments are absent at tree level and they can only show up in higher-order corrections, they turn out to be very small in the SM. Therefore, any deviation could indicate the presence of new physics; on the contrary, consistency with the SM values

---

*Published by the American Physical Society under the terms of the Creative Commons Attribution 4.0 International license. Further distribution of this work must maintain attribution to the author(s) and the published article's title, journal citation, and DOI. Funded by SCOAP<sup>3</sup>.*

could constrain the new couplings that may contribute to this process.

The paper is organized as follows. In Sec. II, we describe an effective field theory approach and define the top-quark CEDM and chromomagnetic dipole moment (CMDM) in this context, and we translate these moments to dimension-six operators. In Sec. III, we explain  $t\bar{t}\gamma\gamma$  production at the LHC within the SM framework, and then use the dimension-six operators via the effective Lagrangian approach to calculate the cross section. In Sec. IV, we explain the signal process selection strategy and consider related background processes. In Sec. V, we discuss the current constraints on  $d_V^q$  and  $d_A^q$  from inclusive top pair production; then, we introduce the new ratio  $R_{2\gamma/\gamma} = \sigma_{t\bar{t}\gamma\gamma}/\sigma_{t\bar{t}\gamma}$  to constrain the anomalous couplings. In Sec. VI, we employ the scalar sum of the jet's transverse momentum distribution to define a signal-dominated region and use a single-bin experiment to extract the limits on  $d_V^q$  and  $d_A^q$ . Finally, in Sec. VII we summarize the results and conclude the paper.

## II. $g\bar{t}t$ EFFECTIVE COUPLING

Effective field theory is a remarkable framework to describe the effects of physics at a high energy scale  $\Lambda$ , which is necessarily higher than the energy scale of the experiment. Essentially, when the heavy degrees of freedom from high-energy physics cannot be directly produced one can integrate them out, resulting in new terms which are added to the SM Lagrangian. These new terms are composed of higher-dimensional operators suppressed by the inverse power of  $\Lambda$ , and they respect Lorentz invariance, SM gauge symmetries, and baryon and lepton number conservation. Thus, the SM effective Lagrangian up to the dimension-six operators can be written as follows:

$$\mathcal{L}_{\text{eff}} = \mathcal{L}_{\text{SM}} + \sum_i \frac{c_i \mathcal{O}_i^{(6)}}{\Lambda^2}, \quad (1)$$

where  $\mathcal{L}_{\text{SM}}$  is the SM Lagrangian.  $\mathcal{O}_i^{(6)}$  are the dimension-six operators (which are the dominant contribution to the experimental observables) and the  $c_i$ 's are unknown dimensionless coefficients that describe the strength of the new physics couplings to the SM particles. After EWSB, the integrated-out terms will produce new couplings that do not exist at tree level in the SM (such as electric and magnetic dipole moments), as well as couplings which correct the SM interactions. The most general form of the  $g\bar{t}t$  coupling assuming up to dimensions-six operators can be depicted as follows:

$$\mathcal{L}_{g\bar{t}t} = -g_s \bar{t} \frac{\lambda^a}{2} \gamma^\mu t G_\mu^a - g_s \bar{t} \frac{\lambda^a}{2} \frac{i\sigma^{\mu\nu}}{m_t} (d_V^q + i d_A^q \gamma_5) t G_{\mu\nu}^a, \quad (2)$$

where  $g_s$ ,  $\lambda^a$ , and  $G_{\mu\nu}^a$  are the strong coupling constant, Gell-Mann matrices, and gluon field-strength tensor,

respectively.  $d_V^q$  and  $d_A^q$  are real parameters which represent the top-quark chromomagnetic and chromoelectric dipole moments. The first term is the SM interaction, while the rest of the terms contain the  $g\bar{t}t$  and  $ggt\bar{t}$  interactions and are generated from dimension-six operators based on the convention used in Refs. [11,12], which have the following form:

$$O_{uG\phi}^{33} \sim (\bar{q}_{L3} \lambda_a \sigma^{\mu\nu} t_R) \tilde{\phi} G_{\mu\nu}^a, \quad (3)$$

where  $\bar{q}_{L3}$  and  $t_R$  are the weak doublet of the left-handed quark field and right-handed top quark field, respectively.  $\phi$  is the weak doublet of the Higgs field and  $\tilde{\phi} = i\tau_2 \phi^*$ . The relation between the dimension-six operator in Eq. (3) and the chromomagnetic moments of the top quark after the symmetry breaking can be written as

$$\delta d_V^q = \frac{\sqrt{2}}{g_s} \text{Re} O_{uG\phi}^{33} \frac{v m_t}{\Lambda^2}, \quad \delta d_A^q = \frac{\sqrt{2}}{g_s} \text{Im} O_{uG\phi}^{33} \frac{v m_t}{\Lambda^2}, \quad (4)$$

where  $m_t$  is the top-quark mass and  $v$  is the vacuum expectation value of the Higgs field. The CEDM and CMDM are related to the real and imaginary parts of  $O_{uG\phi}^{33}$  and both are considered in this study.

In the SM, the CMDM of the top quark ( $d_V^q$ ) can be generated via one-loop QCD and electroweak diagrams. There are two types of Feynman diagrams that contribute to the QCD part. The first diagram is the one with an external gluon emitted from the internal top quark, and in the second diagram the external gluon is comes from the exchanged gluon due to the non-Abelian properties of the strong interaction. The total QCD contribution is  $d_V^q = -0.008$  [13], which is the dominant SM loop contribution. In the electroweak loop diagrams,  $W^\pm$ ,  $Z$ , and Higgs bosons can be exchanged while the gluon can be emitted from the internal quark. This tiny contribution is about 12% of the QCD part but with the opposite sign. Finally, the total SM loop correction is  $d_V^q = -0.007$  [13]. The CEDM contribution in the SM arises from the three-loop diagrams and has been shown to be very small [13].

Direct bounds on the CMDM and CEDM from inclusive and differential measurements of  $t\bar{t}$  processes at the Tevatron and LHC have been obtained [14–21]. Also, with the considerable amount of the data that the LHC in its upgraded phase will collect, the rare SM processes such as  $t\bar{t}$  in association with two heavy gauge bosons and multitop quark production have been shown to be sensitive to these anomalous interactions of the top quark and gluon [5,22]. In addition, the CMS experiment has obtained limits on these dipole moments via the measurement of the  $t\bar{t}$  spin correlation using  $\sqrt{s} = 8$  TeV data [23]. Moreover, it has been shown that there is sufficient sensitivity to probe the CMDM and CEDM given the high invariant mass of top pair processes where top quarks are highly boosted [24].

Single top  $tW$  production has also been shown to be sensitive to top quark chromomagnetic moments via its cross section and top-quark polarization [25,26].

In addition to the direct bounds, there are also indirect bounds on the top-quark dipole moments from low-energy measurements. For example, from the measurement of rare  $B$ -meson decays  $b \rightarrow s\gamma$ , the top-quark chromomagnetic moment constrains at the 95% confidence level (C.L.) with  $-3.8 \times 10^{-3} < d_V^g < 1.2 \times 10^{-3}$  [27]. Also, measurements of the neutron electric dipole moment could constrain the top-quark chromoelectric dipole moment to  $|d_A^g| \leq 0.95 \times 10^{-3}$  at 90% C.L. [18]. In the next sections, we examine the potential of the  $t\bar{t}\gamma\gamma$  process to probe the top-quark CMDM and CEDM.

### III. $t\bar{t}\gamma\gamma$ PRODUCTION IN PROTON-PROTON COLLISIONS

Top-pair production in association with two photons within the SM framework can occur through gluon-gluon fusion or quark-antiquark annihilation at the LHC. The Feynman diagrams with the dominant contribution for the  $t\bar{t}\gamma\gamma$  process are shown in Fig. 1. The reason that the dominant production mode for  $t\bar{t}\gamma\gamma$  is from  $q\bar{q}$  annihilation comes from the fact that photons can radiate either from top quarks or initial-state quarks, while this is not the case for the gluon-gluon fusion production mode. For instance, the calculated contributions of the  $q\bar{q}$  production mode at leading order (LO) with  $\sqrt{s} = 13$  TeV for  $t\bar{t}$ ,  $t\bar{t}\gamma$ , and  $t\bar{t}\gamma\gamma$  processes are 13%, 32%, and 66%, respectively, when the  $p_T$  of the photon is set greater than 10 GeV at the generator level.

We use the MADGRAPH5\_AMC@NLO package [28] for event generation and to calculate the cross sections. The total cross section is calculated assuming a top-quark mass  $m_t = 172.5$  GeV,  $W$ -boson mass  $m_W = 80.37$ , GeV and  $G_F = 1.16639 \times 10^5$  GeV<sup>2</sup>. We use parton distribution functions (PDFs) from the set NNPDF3 [29]. The values of the factorization scale ( $\mu_F$ ) and renormalization scale ( $\mu_R$ ) are calculated event by event and are considered to be  $\mu_F = \mu_R = \sqrt{m_t^2 + \sum_i p_T^2(i)}$ , where the sum is over the visible final-state particles. Top-quark and  $W$ -boson decays are considered in the narrow-width approximation, and spin correlation in the top quarks decay is considered.

To calculate the cross section of  $t\bar{t} + X$  including the chromomagnetic moments of the top quark, the effective Lagrangian is imported via the FEYNRULES package [30] and the obtained Universal FEYNRULES Output model [31] is linked to MADGRAPH5\_AMC@NLO in order to generate events and calculate the cross section. The total calculated cross section at leading order arising from dimension-six operators in Eq. (3), including the CMDM and CEDM of the top quark, is parametrized as

$$\sigma_{\text{total}} = \sigma_{\text{SM}} + \alpha d_V^g + \beta (d_V^g)^2 + \kappa (d_A^g)^2, \quad (5)$$

where  $\sigma_{\text{SM}}$  is the SM cross section. The second term is the interference between the SM and the real part of the  $O_{uG\phi}^{33}$  operator, which has a  $\frac{1}{\Lambda^2}$  contribution. The third and fourth quadratic terms correspond to three pure real and imaginary parts of  $O_{uG\phi}^{33}$ , which have the contributions of the order of  $\frac{1}{\Lambda^4}$ . It should be mentioned that dimension-eight operators also generate additional terms of the order of  $\frac{1}{\Lambda^4}$ , but we drop those terms as we only consider the dimension-six operators in this analysis. In Eq. (5), there is no linear  $d_A^g$  term as the cross section must be a  $CP$ -conserving observable.

In addition to the signal process, we generate several reducible background processes using MADGRAPH5\_AMC@NLO, such as  $t\bar{t}\gamma$ ,  $W\gamma\gamma + \text{jets}$ , single top +  $\gamma\gamma$ ,  $Z\gamma\gamma + \text{jets}$ , diboson +  $\gamma\gamma$  including  $WW\gamma\gamma$ ,  $WZ\gamma\gamma$ , and  $ZZ\gamma\gamma$  and finally  $\gamma\gamma + \text{jets}$ , as well as an irreducible background which is the SM  $t\bar{t}\gamma\gamma$ . All of the generated samples are passed to PYTHIA 8 [32] in order to perform parton showering and hadronization. Jet clustering is performed using the anti- $k_r$  algorithm [33] implemented in the FASTJET package [34] using a radius parameter of  $R = 0.5$ .  $b$ -tagging and mistagging efficiencies for the jets that originate from the hadronization of a  $b$  quark are considered [35]. These efficiencies are parametrized based on the transverse momentum of the jets. In this analysis, the fast detector response is estimated using the DELPHES 3.4.1 package [36] based on the similar conditions of the CMS detector.

### IV. ANALYSIS STRATEGY

In this section, we present the analysis strategy to select the  $t\bar{t}\gamma\gamma$  signal events. We also discuss the relevant

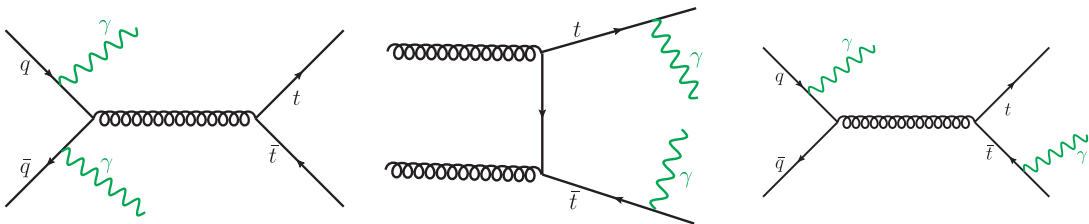


FIG. 1. Dominant Feynman diagrams for  $t\bar{t}$  production in association with two photons within the SM framework.

background processes and estimate their contributions in this final state. As a result, one can obtain the potential power of these processes to probe the chromomagnetic moments of the top quark, which we will discuss in the next sections. In this analysis we consider the semileptonic decay mode of the  $t\bar{t}\gamma\gamma$  process, as this decay mode has the largest contribution and the presence of one lepton along with two photons will help to effectively suppress the background processes.

We select signal events that have exactly two isolated photons with transverse momenta  $p_T > 25$  GeV and pseudorapidity  $|\eta| < 2.5$ . We also require a lepton (electron or muon) with the same  $p_T$  and  $\eta$  cut values as the photons. Moreover, we veto events that contain any other leptons in order to suppress the backgrounds, including  $Z$ -boson events such as  $Z\gamma\gamma + \text{jets}$ . The requirements for jet selection are  $p_T > 40$  GeV and  $|\eta| < 5$ , and the requirements for the  $b$ -tagged jets are  $p_T > 40$  GeV and  $|\eta| < 2.5$ . In order to suppress the backgrounds that do not contain a  $W$  boson, we require the missing transverse energy (MET) to be greater than 30 GeV. In addition to the mentioned cuts, in order to have well-isolated objects we require the angular separation between the two photons and between the photons and other objects to be  $\Delta R(\gamma, X) = \sqrt{\Delta\phi^2 + \Delta\eta^2} > 0.5$  where  $X = e, \mu, \text{jets}, b \text{ jets}, \text{ or } \gamma$ . On top of the other requirements, we require that the events have  $H_T > 300$  GeV, where  $H_T = \Sigma p_T$ , and the sum is performed over the transverse momentum of jets within the defined acceptance region. Higher values of  $H_T$  correspond to the heavier final state masses, which is  $t\bar{t}$  in the case of our signal and could suppress the processes with lower-mass and no-mass states such as  $W + \text{jets} + \gamma\gamma$  and  $\gamma\gamma + \text{jets}$ , respectively. Table I shows the expected yields for the two signal samples  $d_V^g = 0.2$ , and  $d_A^g = 0.2$  as well as the SM backgrounds after applying each set of selection cuts. It should be mentioned that the expected yields for the signal samples comprise the contribution of anomalous top-quark dipole moments, the SM  $t\bar{t}\gamma\gamma$  contribution, and their interference.

Apart from the background processes with two real photons, there is a contribution from the  $t\bar{t}\gamma$  process. First, it should be mentioned that  $t\bar{t}\gamma$  is a different process from  $t\bar{t}\gamma\gamma$  as the latter has two photons in the matrix elements while the former has one. However, events from the  $t\bar{t}\gamma$  process

may have overlap with  $t\bar{t}\gamma\gamma$  when the photon radiated from PYTHIA parton shower lands into the generator acceptance of  $t\bar{t}\gamma\gamma$ . Due to the high cut value applied for  $\Delta R$  between the photons and other objects, one would expect this overlap to be small. However, we have subtracted this contribution in order to be precise in our background estimation. The total obtained yield for  $t\bar{t}\gamma$  after applying all of the selection cuts is 14 for  $100 \text{ fb}^{-1}$ .

In addition to the above background processes, in the real experiment there is a probability that the jets are misidentified as a photon. The reason behind this misidentification is that inside a jet there is a considerable amount of neutral hadrons such as pions which promptly decay into the two photons in the boosted topology. Therefore, the produced shower of these two close-by photons will overlap inside the electromagnetic calorimeter and be misidentified as a photon, a so-called ‘‘fake’’ photon. As a result, in a real detector processes with large cross sections, such as  $W/Z + \text{jets}$ ,  $W/Z + \text{jets} + \gamma$ , multijet  $+ \gamma$ , and multijet, may pass our selection criteria due to this misreconstruction of jets. In real experiments such as CMS and ATLAS the probability of jet-to-photon misreconstruction  $P_{j \rightarrow \gamma}$  varies between  $10^{-3}$ – $10^{-5}$  depending on the transverse momentum and pseudorapidity of a photon. We have estimated the contribution of these processes by applying the selection cuts explained in the Table I except the selection cuts on the photons. Then, the resulting cross sections are multiplied by  $P_{j \rightarrow \gamma}$  or  $P_{j \rightarrow \gamma}^2$  according to the number of misreconstructed photons for each process. The contribution of these processes is found to be negligible. However, a precise estimation of fake photons is usually performed using data-driven techniques and a full simulation of detector components, which is beyond the scope of this analysis.

## V. THE $t\bar{t}\gamma\gamma$ PROCESS’S ROLE IN CONSTRAINING THE STRONG DIPOLE MOMENTS OF THE TOP QUARK

In this section we explain how the  $t\bar{t}\gamma\gamma$  process can play a complementary role in constraining the chromomagnetic moments of the top quark. First we discuss the current bounds that one can obtain from the inclusive cross section measurements of  $t\bar{t} + X$ , where  $X = \gamma$  or jets. Then, in the second part we discuss the constraints from the newly

TABLE I. Expected number of events for the two signal samples and backgrounds after applying the selection cuts for  $100 \text{ fb}^{-1}$  IL.

$\sqrt{s} = 13 \text{ TeV}, 100 \text{ fb}^{-1} \text{ IL}$ Selection cuts	Signal + $t\bar{t}\gamma\gamma$		Backgrounds with two real photons				
	$d_V^g = 0.2$	$d_A^g = 0.2$	$t\bar{t}\gamma\gamma$	$W/Z + \text{jets}\gamma\gamma$	Single $\text{top}\gamma\gamma$	diboson $\gamma\gamma$	jets $\gamma\gamma$
$p_{T,\text{lep}}, \eta_{\text{lep}} \quad N_{\text{lep}} = 1, \text{ lepton and } \gamma \text{ veto}$	305	582	206	1834	239	6491	$1.36 \times 10^5$
$p_{T,\gamma}, \eta_\gamma, \quad N_\gamma = 2$	47	87	29	147	39	50	281
$p_{T,\text{jets},b \text{ jets}}, \eta_{\text{jets},b \text{ jets}}, \quad N_{\text{jets}} > 1,$ $N_{b \text{ jets}} = 2, \text{ MET}, H_T, \Delta R(\gamma, X)$	7.15	10.20	3.01	0.03	0.44	0.09	0

TABLE II. Values of  $\alpha$ ,  $\beta$ , and  $\kappa$  for the Tevatron and LHC. The SM cross sections are inclusive ones except for the  $t\bar{t}\gamma$  process which is presented per semileptonic final state.

Process	$\sigma_{\text{SM}}[pb]$	$\alpha$	$\beta$	$\kappa$
$t\bar{t}$ Tevatron $\sqrt{s} = 1.96$ TeV	$7.35 \pm 0.21$	-55.9	164	64
$t\bar{t}$ LHC $\sqrt{s} = 8$ TeV	$252.8 \pm 14.4$	-1668	9013	7828
$t\bar{t}$ LHC $\sqrt{s} = 13$ TeV	$832 \pm 43$	-5395	31387	27400
$t\bar{t}\gamma$ LHC $\sqrt{s} = 8$ TeV	$0.592 \pm 0.077$	-3.39	18.75	13.98

defined ratio  $\sigma_{t\bar{t}\gamma}/\sigma_{t\bar{t}\gamma}$  and the possible improvements with respect to inclusive  $t\bar{t}$  cross section measurements.

### A. Constraints from $t\bar{t} + X$ production measurements

In order to obtain stringent bounds on  $d_V^g$  and  $d_A^g$  one could combine results from different experiments. In this section we consider the measurements on the inclusive cross sections of  $t\bar{t}$  at the Tevatron from  $p\bar{p}$  collisions at  $\sqrt{s} = 1.96$  TeV [37], the combined measurements of  $pp$  collisions at CMS and ATLAS with  $pp$   $\sqrt{s} = 8$  TeV [38], and two other recent measurements at CMS on the cross section of  $t\bar{t}\gamma$  at  $\sqrt{s} = 8$  TeV [9] and the cross section of  $t\bar{t}$  at  $\sqrt{s} = 13$  TeV [39].

In order to obtain the experimental bounds, one needs to calculate the functionality of the total cross section to the anomalous couplings based on the particles that collide and the center-of-mass energy of collisions. Exploiting the method explained in Sec. III, we evaluate the total cross sections including the leading-order contribution of top quark chromomagnetic moments. Table II shows the obtained values for each coefficient belonging to the linear and quadratic terms for each measurement. The constraints on the anomalous couplings obtained using the measured

cross sections along with the precise available cross sections that the SM predicts at next-to-leading order or next-to-next-to-leading order (NNLO) calculated with TOP++ [40]. In order to obtain the limit bands we consider the total uncertainty of the cross sections measured in Refs. [9,37–39], as well as the theoretical uncertainties on the predicted cross sections including the PDF, renormalization/factorization scales, and top-quark mass uncertainties. The theoretical uncertainties for the  $t\bar{t}$  cross section at NNLO (calculated in Ref. [40]) arising from scale variations and  $(\text{PDF} + \alpha_s)$  are 3 and 5% for  $\sqrt{s} = 8$  TeV, 3 and 4% for  $\sqrt{s} = 13$  TeV, and 2 and 2% for  $\sqrt{s} = 1.96$  TeV, respectively. The left panel of Fig. 2 depicts the two-dimensional bounds on  $d_V^g$  and  $d_A^g$  for each measurement separately, and the right panel shows the overlap region of all measurements. The total colorful area is the bound obtained at Tevatron and LHC8, which is compatible with the results of Refs. [15,24]. The pink area is the bound obtained by adding CMS13  $t\bar{t}$  cross section measurements with  $2.2 \text{ fb}^{-1}$  integrated luminosity and the  $t\bar{t} + \gamma$  measurement at CMS at a center-of-mass energy of 8 TeV. As can be seen, the bounds' improvement is not significant and is only for the  $d_V^g$  coupling. The  $t\bar{t} + \gamma$  measurement also does not produce tighter bounds. As the  $t\bar{t}$  inclusive cross section measurement at CMS13 is systematically dominated, adding more data recorded by CMS in 2016 will not increase the precision of the measurements by a large value, and consequently no big improvement in the bounds of the top-quark dipole moments is expected. Moreover, one can show that considering better precision of the inclusive cross section only leads to obtaining better bounds on  $d_V^g$ . Therefore, we introduce a new observable to the selected phase space which provides a different functionality and can be used to tighten the current bounds, especially on  $CP$ -violating couplings.

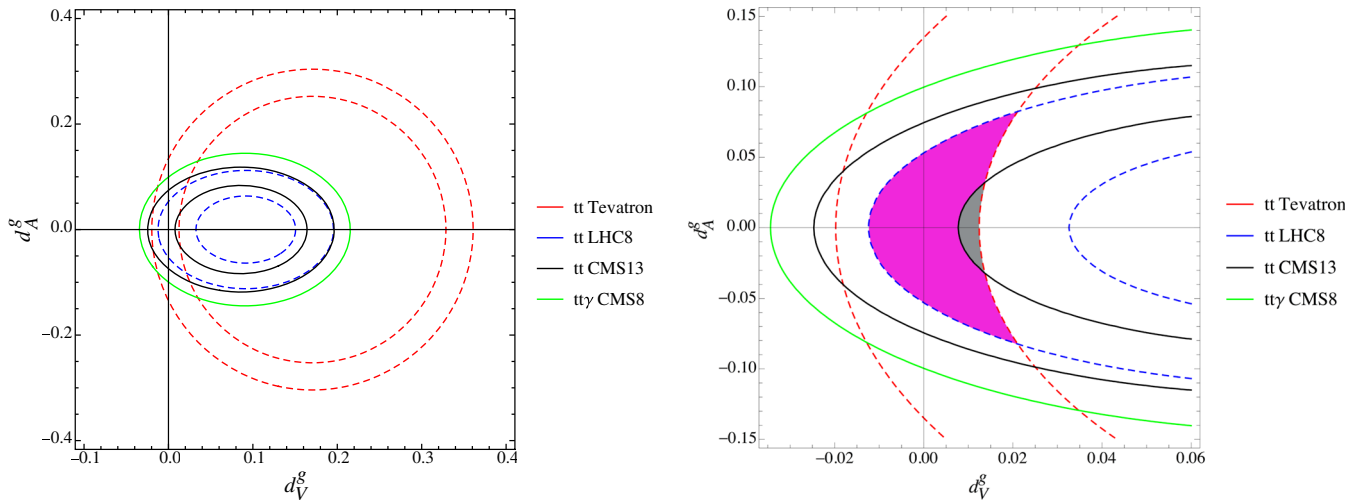


FIG. 2. Two-dimensional allowed regions for  $d_V^g$  and  $d_A^g$  using the different measurements that have been performed so far. The left panel shows each experimental bound and the right panel depicts the overlap region.

## B. Cross section ratio

As discussed in the previous section, the current cross section measurements of top-quark pair production have a limited ability to tighten the current bounds on top-quark chromomagnetic moments. Therefore, we propose a new observable which is the cross section ratio of  $t\bar{t}\gamma\gamma$  to  $t\bar{t}\gamma$  within a selected phase space in order to constrain the currently allowed region of these anomalous couplings. It is defined as

$$R_{2\gamma/\gamma} = \sigma_{t\bar{t}\gamma\gamma} / \sigma_{t\bar{t}\gamma}, \quad (6)$$

where the numerator and denominator are calculated in the same signal region except for the required number of photons, which is two for the numerator and one for the denominator. Using this ratio has the advantage of canceling the systematic uncertainties. From the theoretical point of view, uncertainties from the parton distribution function and  $\alpha_s$  can be reduced. Apart from that, several systematic uncertainties arising from the luminosity, jet energy scale,  $b$ -jet tagging, and lepton identification can be canceled out. In particular, using the proposed  $R_{2\gamma/\gamma}$  will effectively reduce the photon identification uncertainties as well.

Several studies have studied the idea of using the cross section ratio in order to reduce the uncertainties. For instance, in Ref. [41] the authors showed that by using the ratio  $\sigma_{t\bar{t}+H} / \sigma_{t\bar{t}+Z}$  the top Yukawa coupling can be measured with 1% precision using proton-proton collision data with a center-of-mass energy of 100 TeV. In another study it was shown that at the LHC the cross section ratio of single top quark production in association with a photon over single top quark production  $\sigma_{tj\gamma} / \sigma_{tj}$  is a precise observable that can probe the top-quark electric and magnetic dipole moments [42]. Also, it has been shown that using  $\sigma_{t\bar{t}+\gamma} / \sigma_{t\bar{t}}$  and  $\sigma_{t\bar{t}+Z} / \sigma_{t\bar{t}}$  could cancel several sources of uncertainties, and these ratios may be more sensitive observables of the electroweak dipole operators of the top quark [43]. The available measurements on the cross section ratio  $\sigma_{t\bar{t}+\gamma} / \sigma_{t\bar{t}}$  at the Tevatron and LHC and the measured cross section of a single top quark in association with a photon can be found in Refs. [8,9,44,45].

We test  $R_{2\gamma/\gamma}$  against the variation of renormalization and factorization scales by generating dedicated samples considering  $\mu_f = \mu_R$  and equate them first to  $2 \times Q_0$  and then to  $Q_0/2$ . Then the ratios for each value of  $\mu_f = \mu_R$  are calculated respectively. The uncertainty due to this scale variation of  $R_{2\gamma/\gamma}$  is obtained below  $\pm 0.5\%$ , while the uncertainty for each total cross section is about 12%. We also evaluate the robustness of these ratios against the variation of PDFs by generating different samples for  $t\bar{t}\gamma\gamma$  and  $t\bar{t}\gamma$  using the three different PDF sets NNPDF3.0 [46], MSTW08 [47], and CTEQ6L1 [48]. Then, we calculate the ratio  $R_{2\gamma/\gamma}$  for each set of PDFs, which results in an uncertainty of about 2%. The stability of this ratio against

different uncertainties shows that this is a robust experimental observable.

In the following, we discuss the effect of these anomalous couplings on the defined ratio. As explained in Sec. III, the contribution of gluon-gluon fusion to  $t\bar{t}\gamma\gamma$  is lower than the  $t\bar{t} + \gamma$  and  $t\bar{t}$  processes, considering that photon radiation from this initial state is forbidden. Thus, the ratio  $R_{2\gamma/\gamma}$  benefits from this dissimilar functionality and can probe these anomalous couplings in a region that is different from the one obtained from the normal inclusive cross section. Considering the  $3 \text{ ab}^{-1}$  of integrated luminosity expected to be delivered by the LHC and the cancellation of different sources of uncertainty, this ratio in the selected phase space can be measured with very good precision. Therefore, we consider two total uncertainties, 5% and 10%, and extract the two-dimensional 95% bounds on  $d_V^g$  and  $d_A^g$ . The left panel of Fig. 3 shows the 95% C.L. allowed regions extracted from different measurements (dashed lines) compared to those obtained from  $R_{2\gamma/\gamma}$  with a 5% uncertainty (solid blue lines). The right panel of Fig. 3 compares the current combined limit obtained from the Tevatron and LHC at 8 and 13 TeV (shaded gray area) with the bound obtained using  $R_{2\gamma/\gamma}$  with a 5% uncertainty. It can be seen that the new behavior of this ratio can tighten the currently allowed region for both anomalous couplings; in particular, it has a considerable ability to constrain  $d_A^g$ . The obtained bounds using  $R_{2\gamma/\gamma}$  for each coupling are  $-0.0088 < d_V^g < 0.0083$  and  $-0.037 < d_A^g < 0.037$  assuming a 5% uncertainty, and  $-0.0177 < d_V^g < 0.0164$  and  $-0.050 < d_A^g < 0.050$  assuming a 10% total uncertainty. It should be mentioned that the reported bounds of each coupling are obtained when the other one is set to zero.

## VI. KINEMATIC HANDLE

In this section, we explore the sensitivity of the  $t\bar{t}\gamma\gamma$  process to probe the top-quark CMDM and CEDM by looking into the kinematic distribution of final-state particles. Equation (2) indicates that additional terms originating from dimension-six operators have a different Lorentz structure as well as particular dependences on the field's momentum. Thus, one expects that the rate and kinematic distribution of final-state particles will be altered due to the presence of such anomalous couplings.

Figure 4 we show some normalized kinematic distributions to compare the expected SM  $t\bar{t}\gamma\gamma$  process with the same process when we apply only either  $d_V^g = 0.3$  or  $d_A^g = 0.3$ . The top left show the  $H_T$  distribution, and the top right and bottom plots show the missing transverse energy and invariant mass of two photons, respectively. Figure 4 indicates that including the new terms in the effective Lagrangian modifies the shape of these distributions, especially in the tail of distributions where the process happens at higher energy scale and shows the momentum

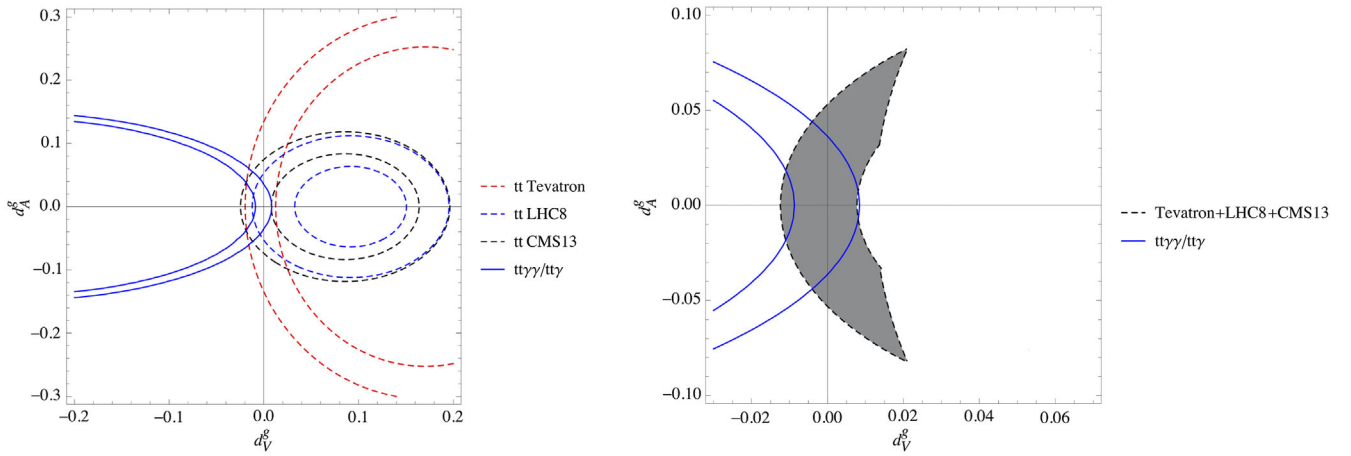


FIG. 3. Left: Comparison of the current obtained bounds from the Tevatron and LHC at 8 and 13 TeV using inclusive top-pair production with the extracted 95% C.L. allowed region obtained from  $R_{2\gamma/\gamma}$  assuming a 5% uncertainty in the selected phase space. Right: A zoomed-in view of the overlap region, showing the improvement in the obtained constraints from  $R_{2\gamma/\gamma}$ .

dependence of these anomalous couplings. It should be mentioned that these plots include the effects of showering, hadronization, and object clustering, and detector effects.

We use the  $H_T$  distribution as a sensitive observable to find the potential upper limit on the cross section of  $t\bar{t}\gamma\gamma$

in the presence of  $d_V^g$  and  $d_A^g$ , and then use this upper limit to obtain the constraint on these couplings assuming that no deviation from the SM is observed. We use a single-bin counting experiment over the  $H_T$  distribution in the signal region which is the region with high values

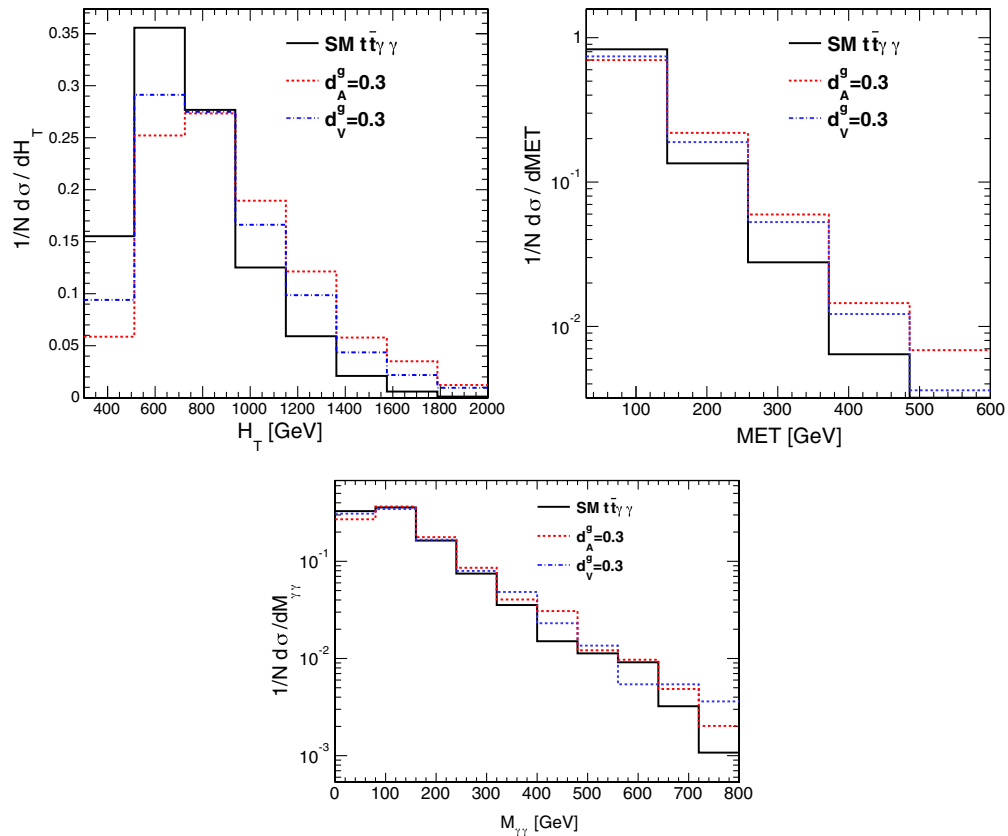


FIG. 4. Normalized distributions of  $H_T$ , missing transverse energy, and invariant mass of two photons. The plots compare the SM  $t\bar{t}\gamma\gamma$  process with the same process when only either  $d_V^g$  or  $d_A^g$  is applied.

of  $H_T$ . Essentially, this signal region has to be optimized for the best cut value of  $H_T$ . The conventional criteria are to obtain the value which results in the lowest limit on the cross section or, in the other words, the best power that bounds  $d_V^g$  and  $d_A^g$ . Therefore, one needs to minimize the 95% expected limit on the signal cross section in order to find the optimized  $H_T$  value. It is worth mentioning that in the optimization procedure one needs only to consider the statistical uncertainty, and no systematic uncertainty is applied. The statistical procedure to extract the expected limit is as follows. The probability of measuring  $N$  events in the signal region is given by a Poisson distribution,

$$P(N|\sigma_{\text{sig}}\varepsilon\mathcal{L}, B) = e^{-(B+\sigma_{\text{sig}}\varepsilon\mathcal{L})} \frac{(B+\sigma_{\text{sig}}\varepsilon\mathcal{L})^N}{N!}, \quad (7)$$

where  $\sigma_{\text{sig}}$ ,  $\mathcal{L}$ ,  $\varepsilon$ , and  $B$  are the signal cross section, integrated luminosity, signal efficiency, and number of expected background events, respectively. These parameters are known except for the signal cross section, which is the parameter of interest. The signal efficiency in the signal region is defined as the number of events passing our selection cuts (explained in Sec. IV) and a certain cut value of  $H_T$  over the total number of events that only pass the  $H_T$  cut. Exploiting the Bayesian approach, one can extract the 95% C.L. upper limit on the signal cross section in the signal region by integrating over the posterior probability, defined as

$$0.95 = \frac{\int_0^{\sigma_{\text{sig}}^{95\%}} P(N|\sigma_{\text{sig}}\varepsilon\mathcal{L}, B)d\sigma_{\text{sig}}}{\int_0^{\infty} P(N|\sigma_{\text{sig}}\varepsilon\mathcal{L}, B)d\sigma_{\text{sig}}}. \quad (8)$$

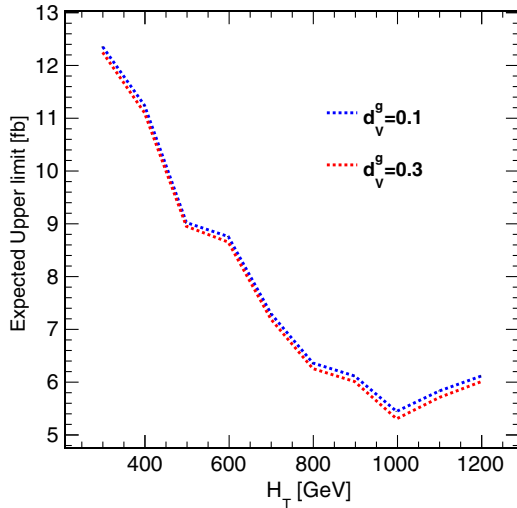


FIG. 5. The 95% expected limit on the cross section as a function of  $H_T$  for two different values of  $d_V^g$  is shown. The optimized  $H_T$  value is found to be 1000 GeV considering 100  $\text{fb}^{-1}$  IL.

This statistical tool is employed to find the optimized cut value for  $H_T$ . Therefore, we calculate the 95% C.L. expected limits on the cross section for different values of  $H_T$ , ranging from 400 to 1200 GeV in steps of 100 GeV. The optimization is done for only one of the couplings while the other coupling is set to zero. This procedure is also performed for different values of each coupling to see if any dependence on the coupling parameter exists. Figure 5 shows the 95% expected limit as a function of  $H_T$  for  $d_V^g = 0.1, 0.3$  considering 100  $\text{fb}^{-1}$  IL.

The minimum expected limit is obtained for  $H_T = 1000$  GeV. The same procedure is implemented for  $d_A^g = 0.1, 0.3$  and the same optimized value is obtained. Therefore, we consider the signal region by applying the selection cuts and  $H_T > 1000$  GeV assuming 100  $\text{fb}^{-1}$  of data.

In the limit calculation procedure we consider the statistical and systematic uncertainties due to the SM background processes. Given that most of these backgrounds have not been measured and we generate them at leading order, we assume 100% uncertainty on the background yields in the signal region.

We find the limits on  $d_V^g$  and  $d_A^g$  by comparing the expected limit on the cross section with the theoretical cross section in the signal region considering 100 and 300  $\text{fb}^{-1}$  at  $\sqrt{s} = 13$  TeV and 3000  $\text{fb}^{-1}$  at  $\sqrt{s} = 14$  TeV. It should be mentioned that the compared theoretical cross section curves in the signal region are subtracted from the SM value to consider the pure non-SM cross sections originated by dimension-six operators. The results obtained for the different integrated luminosities and different center-of-mass energies are shown in Table III.

Figure 6 shows the upper limits on  $d_V^g$  (left) and  $d_A^g$  (right) considering 300  $\text{fb}^{-1}$  IL, which are compared with the theoretical curves. The obtained bounds from the  $H_T$  distribution show very good improvement using the 3000  $\text{fb}^{-1}$  expected amount of data, especially for the  $d_A^g$  coupling. It should be mentioned that in general the optimized cut value changes when one assumes different integrated luminosities. Thus, in order to obtain the limit for each considered amount of data, the optimization procedure is performed separately.

TABLE III. Obtained limit on  $d_V^g$  and  $d_A^g$  considering 100, 300, and 3000  $\text{fb}^{-1}$  IL.

Integrated luminosity	$d_V^g$	$d_A^g$
100 $\text{fb}^{-1}$ (13 TeV)	[-0.14, 0.19]	[-0.18, 0.18]
300 $\text{fb}^{-1}$ (13 TeV)	[-0.10, 0.15]	[-0.13, 0.13]
3000 $\text{fb}^{-1}$ (14 TeV)	[-0.006, 0.03]	[-0.014, 0.014]

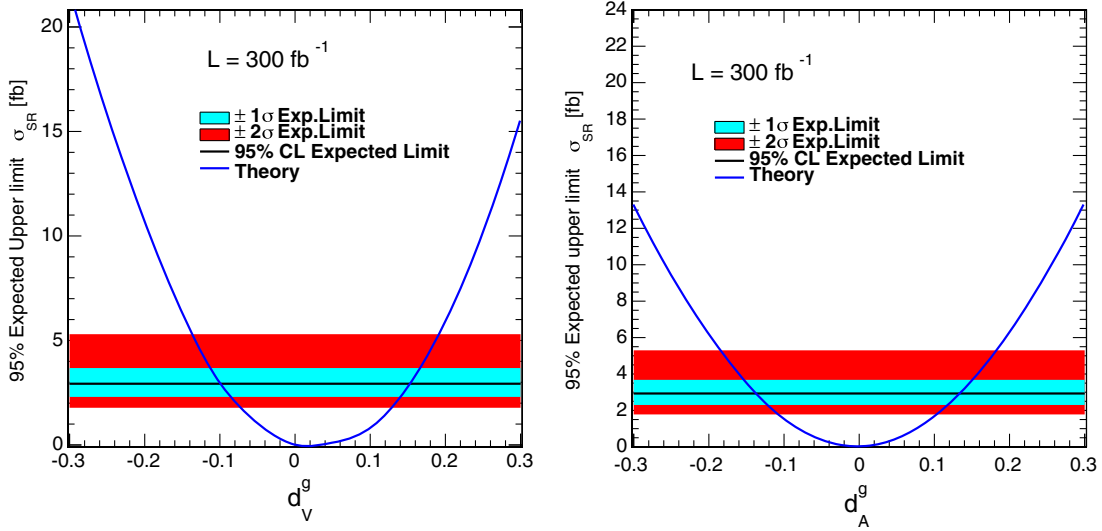


FIG. 6. 95% C.L. expected upper limits on the signal cross section in the signal-dominated region compared with the theoretical cross sections of the signal for 300 fb<sup>-1</sup> IL.

VII. SUMMARY

For the first time, rare SM top quark pair production in association with two photons at the LHC has been considered to investigate the prospects of constraining the top-quark chromomagnetic moments. In the SM, these dipole moments are produced through the higher QCD, electroweak loop corrections, which results in tiny values, and any deviation from SM values would be a hint for new physics. In addition, using processes high particle multiplicity helps to effectively reduce the number of backgrounds. The analysis was performed based on the effective Lagrangian approach where the dimension-six operators induced modifications to the  $gt\bar{t}$  coupling. We considered the semileptonic decay of a top quark pair and defined a set of selection cuts to reconstruct this final state.

Then, a new cross section ratio in the selected phase space,  $R_{2\gamma/\gamma} = \sigma_{t\bar{t}\gamma\gamma}/\sigma_{t\bar{t}\gamma}$ , was introduced. This ratio is important in dealing with the top-quark couplings for two reasons. First, in this observable, a considerable amount of theoretical and experimental uncertainties cancel out. In addition to the conventional reduction of uncertainties, the one related to photon identifications could be reduced due to the presence of a photon in both the numerator and denominator. Second, due to the different contributions of the gluon-gluon production mode in the  $t\bar{t}\gamma\gamma$  and  $t\bar{t}\gamma$  processes, the ratio can probe the different phase spaces of top quark couplings and effectively constrain the  $CP$ -violating coupling  $d_A^g$ . Considering a 5% precision on this ratio measurement, we obtained the limits  $-0.0088 < d_V^g < 0.0083$  and  $-0.037 < d_A^g < 0.037$ .

We also explored different kinematic distributions of parton final-state particles, which include the effects of parton

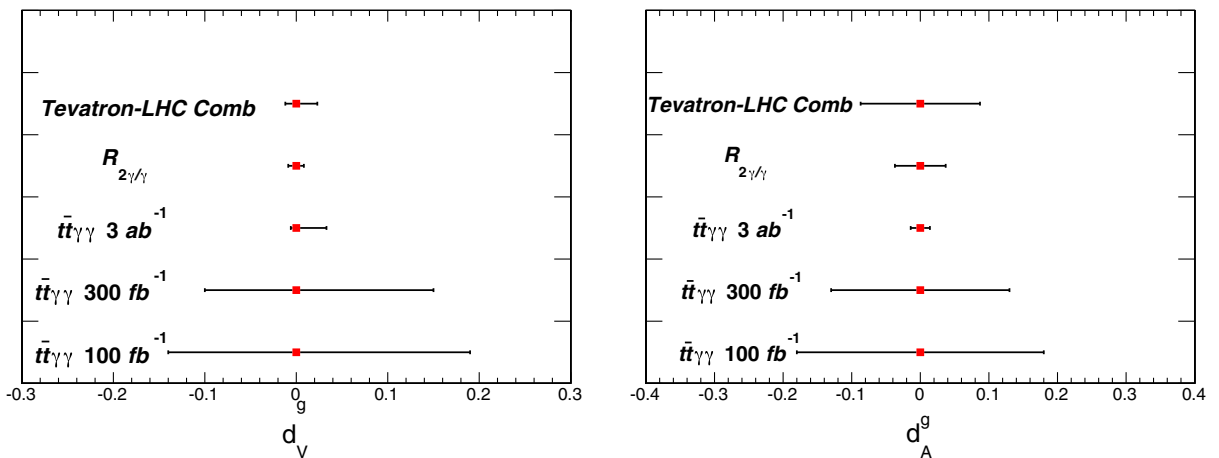


FIG. 7. Summary of the limits for  $d_V^g$  (left) and  $d_A^g$  (right) obtained with the different observables introduced in this analysis assuming different integrated luminosities and the combined results from the Tevatron and LHC8.

showering, hadronization, jet clustering, and detector simulation. We selected the distribution of the scalar sum of jet transverse energy,  $H_T$ . The contribution of these non-SM couplings to higher values of  $H_T$  is pronounced with respect to the pure SM contribution due to the dependence of the new couplings on the momentum. We have optimized the  $H_T$  cut value in order to define a signal region where the best power to probe these couplings is obtained. Finally, we used a counting bin experiment method based on the Bayesian approach to find the upper limit on the signal cross section in the signal region. By comparing the theoretical cross section and upper limit in the defined signal region, we extracted the

bounds  $-0.006 < d_V^g < 0.03$  and  $-0.014 < d_A^g < 0.014$  using  $3 \text{ ab}^{-1}$  IL. Figure 7 shows the summary of the limits for  $d_V^g$  (left) and  $d_A^g$  (right) obtained with the different observables introduced in this analysis, assuming different integrated luminosities and the combined results from the Tevatron and LHC8.

## ACKNOWLEDGMENTS

We thank M. Mohammadi and S. Khatibi for their fruitful discussion, comments, and help in implementing the model.

- 
- [1] ATLAS, CDF, CMS, and D0 Collaborations, [arXiv:1403.4427](#).
- [2] G. Aad *et al.* (ATLAS Collaboration), *Phys. Lett. B* **716**, 1 (2012).
- [3] S. Chatrchyan *et al.* (CMS Collaboration), *Phys. Lett. B* **716**, 30 (2012).
- [4] F. Maltoni, D. Pagani, and I. Tsinikos, *J. High Energy Phys.* **02** (2016) 113.
- [5] S. M. Etesami, S. Khatibi, and M. M. Najafabadi, *Phys. Rev. D* **97**, 075023 (2018).
- [6] M. Aaboud *et al.* (ATLAS Collaboration), *Eur. Phys. J. C* **77**, 40 (2017).
- [7] A. M. Sirunyan *et al.* (CMS Collaboration), *J. High Energy Phys.* **08** (2018) 011.
- [8] G. Aad *et al.* (ATLAS Collaboration), *Phys. Rev. D* **91**, 072007 (2015).
- [9] A. M. Sirunyan *et al.* (CMS Collaboration), *J. High Energy Phys.* **10** (2017) 006.
- [10] M. Aaboud *et al.* (ATLAS Collaboration), *Eur. Phys. J. C* **79**, 382 (2019).
- [11] W. Buchmuller and D. Wyler, *Nucl. Phys.* **B268**, 621 (1986).
- [12] J. A. Aguilar-Saavedra, *Nucl. Phys.* **B812**, 181 (2009).
- [13] R. Martinez, M. A. Perez, and N. Poveda, *Eur. Phys. J. C* **53**, 221 (2008).
- [14] Z. Hioki and K. Ohkuma, *Eur. Phys. J. C* **65**, 127 (2010).
- [15] Z. Hioki and K. Ohkuma, *Phys. Rev. D* **88**, 017503 (2013).
- [16] Z. Hioki and K. Ohkuma, *Phys. Rev. D* **83**, 114045 (2011).
- [17] H. Hesari and M. Mohammadi Najafabadi, *Mod. Phys. Lett. A* **28**, 1350170 (2013).
- [18] J. F. Kamenik, M. Papucci, and A. Weiler, *Phys. Rev. D* **85**, 071501 (2012); **88**, 039903(E) (2013).
- [19] J. A. Aguilar-Saavedra *et al.*, [arXiv:1802.07237](#).
- [20] D. B. Franzosi and C. Zhang, *Phys. Rev. D* **91**, 114010 (2015).
- [21] O. B. Bylund, F. Maltoni, I. Tsinikos, E. Vryonidou, and C. Zhang, *J. High Energy Phys.* **05** (2016) 052.
- [22] M. Malekhosseini, M. Ghominejad, H. Khanpour, and M. M. Najafabadi, *Phys. Rev. D* **98**, 095001 (2018).
- [23] CMS Collaboration, CERN Report No. CMS-PAS-TOP-14-005, 2014.
- [24] J. A. Aguilar-Saavedra, B. Fuks, and M. L. Mangano, *Phys. Rev. D* **91**, 094021 (2015).
- [25] S. Y. Ayazi, H. Hesari, and M. M. Najafabadi, *Phys. Lett. B* **727**, 199 (2013).
- [26] S. D. Rindani, P. Sharma, and A. W. Thomas, *J. High Energy Phys.* **10** (2015) 180.
- [27] R. Martinez and J. A. Rodriguez, *Phys. Rev. D* **65**, 057301 (2002).
- [28] J. Alwall, R. Frederix, S. Frixione, V. Hirschi, F. Maltoni, O. Mattelaer, H.-S. Shao, T. Stelzer, P. Torrielli, and M. Zaro, *J. High Energy Phys.* **07** (2014) 079.
- [29] R. D. Ball *et al.* (NNPDF Collaboration), *J. High Energy Phys.* **04** (2015) 040.
- [30] A. Alloul, N. D. Christensen, C. Degrande, C. Duhr, and B. Fuks, *Comput. Phys. Commun.* **185**, 2250 (2014).
- [31] C. Degrande, C. Duhr, B. Fuks, D. Grellscheid, O. Mattelaer, and T. Reiter, *Comput. Phys. Commun.* **183**, 1201 (2012).
- [32] T. Sjostrand, S. Mrenna, and P. Z. Skands, *Comput. Phys. Commun.* **178**, 852 (2008).
- [33] M. Cacciari, G. P. Salam, and G. Soyez, *J. High Energy Phys.* **04** (2008) 063.
- [34] M. Cacciari, G. P. Salam, and G. Soyez, *Eur. Phys. J. C* **72**, 1896 (2012).
- [35] A. M. Sirunyan *et al.* (CMS Collaboration), *J. Instrum.* **13**, P05011 (2018).
- [36] J. de Favereau, C. Delaere, P. Demin, A. Giammanco, V. Lemaître, A. Mertens, and M. Selvaggi (DELPHES 3 Collaboration), *J. High Energy Phys.* **02** (2014) 057.
- [37] T. A. Aaltonen *et al.* (CDF and D0 Collaborations), *Phys. Rev. D* **89**, 072001 (2014).
- [38] ATLAS Collaboration, CERN Report No. ATLAS-CONF-2014-054, 2014.
- [39] A. M. Sirunyan *et al.* (CMS Collaboration), *J. High Energy Phys.* **09** (2017) 051.
- [40] M. Czakon and A. Mitov, *Comput. Phys. Commun.* **185**, 2930 (2014).
- [41] M. L. Mangano, T. Plehn, P. Reimitz, T. Schell, and H. S. Shao, *J. Phys. G* **43**, 035001 (2016).

- [42] S. M. Etesami, S. Khatibi, and M. M. Najafabadi, *Eur. Phys. J. C* **76**, 533 (2016).
- [43] M. Schulze and Y. Soreq, *Eur. Phys. J. C* **76**, 466 (2016).
- [44] T. Aaltonen *et al.* (CDF Collaboration), *Phys. Rev. D* **84**, 031104 (2011).
- [45] A. M. Sirunyan *et al.* (CMS Collaboration), *Phys. Rev. Lett.* **121**, 221802 (2018).
- [46] R. D. Ball *et al.* (NNPDF Collaboration), *J. High Energy Phys.* **04** (2015) 040.
- [47] A. D. Martin, W. J. Stirling, R. S. Thorne, and G. Watt, *Eur. Phys. J. C* **63**, 189 (2009).
- [48] J. Pumplin, D.R. Stump, J. Huston, H.L. Lai, P.M. Nadolsky, and W.K. Tung, *J. High Energy Phys.* **07** (2002) 012.